



Cite this: *Phys. Chem. Chem. Phys.*, 2025, 27, 20493

A multi-component density functional study on quantum effects of hydrogen nuclei on ground-state and excited-state proton transfer reactions in 7-hydroxyquinoline

Taro Udagawa,^a Hinata Nagasaka,^a Yusuke Kanematsu,^{*b} Takayoshi Ishimoto^b and Masanori Tachikawa^c

The proton transfer (PT) reaction in 7-hydroxyquinoline (7-HQ), mediated by three methanol molecules, has been investigated using time-dependent density functional theory (TD-DFT) and multi-component DFT (MC_TD-DFT) calculations, which can incorporate nuclear quantum effects (NQEs) of protons and deuterons. The NQEs were found to induce the geometrical changes in both the ground-state and excited-state, and alter orbital energies, affecting the HOMO–LUMO energy gap and absorption and fluorescence properties. The MC_DFT calculations predict a Stokes shift of 217 nm, closer to the experimental value (180–200 nm) compared to the conventional DFT (242 nm). For 7-HQ, the NQEs induced red shifts in absorption peaks and blue shifts in fluorescence peaks, aligning the Stokes shift more closely with experimental data. In addition, the MC_DFT calculations revealed that geometrical relaxation induced by the NQEs can be attributed to the shifts in the peaks in the case of 7-HQ. This study highlights the critical role of NQEs in understanding PT mechanisms, absorption and fluorescence properties, and H/D isotope effects, demonstrating the importance of including NQEs for accurate theoretical modeling.

Received 12th July 2025,
Accepted 11th September 2025

DOI: 10.1039/d5cp02666k

rsc.li/pccp

1. Introduction

Hydrogen bonds¹ play a crucial role not only in water, which is indispensable to us, but also in materials such as hydrogen-bonded ferroelectrics,² and in the field of biochemistry, including the formation of the DNA double-helix structure and the higher-order structures of proteins. Furthermore, proton transfer (PT) reactions are fundamental chemical processes that play a critical role in various chemical reaction mechanisms.^{3,4} Among them, excited-state multiple PT (ESMPT) reactions mediated by solvent molecules, as observed in molecules such as 7-hydroxyquinoline (7-HQ),^{5–10} are closely associated with photochemistry and the functional expression of biomolecules. Due to their large Stokes shifts, they also hold significant potential for applications in fluorescent probes and related fields. Given this background, excited-state PT (ESPT) reactions

have been vigorously pursued through experimental and theoretical techniques.^{11–21} There exist many molecules that possess both a proton donor group and a proton acceptor atom, exhibiting ESMPT through hydrogen-bond chains with solvent molecules. Among them, 7-HQ is the most widely used representative molecule for fundamental studies.^{10,22–29}

Density functional theory (DFT) has become the *de facto* standard in quantum chemical calculations today due to its ability to deliver accurate results within reasonable computational times. Time-dependent DFT (TD-DFT), an extension of DFT, is the method of choice for theoretically analyzing excited-states, and numerous studies on ESPT using the TD-DFT approach have been reported.^{5–7,11–20} In general quantum chemical computations, the Born–Oppenheimer (BO) approximation is applied. This approximation assumes that the nuclei, which are much heavier than electrons, are fixed, and thus it only addresses the behavior of electrons in the field created by these fixed nuclei. However, in systems like ESMPT, where hydrogen atoms play a central role, it is often crucial to directly consider the quantum effects of the hydrogen nuclei themselves—known as nuclear quantum effects (NQEs). Although theoretical calculations based on the BO approximation have been successful in analyzing many chemical phenomena, they struggle with systems where NQEs are significant.

^a Department of Chemistry and Biomolecular Science, Faculty of Engineering, Gifu University, Yanagido 1-1, Gifu 501-1193, Japan. E-mail: udagawa.taro.f1@f.gifu-u.ac.jp

^b Smart Innovation Program, Graduate School of Advanced Science and Engineering, Hiroshima University, 1-4-1 Kagamiyama, Higashi-Hiroshima, Hiroshima 739-8527, Japan. E-mail: ykanem@hiroshima-u.ac.jp

^c Graduate School of NanobioScience, Yokohama City University, 22-2 Seto, Kanazawa-ku, Yokohama 236-0027, Japan

In recent years, we have developed the multi-component quantum mechanics (MC_QM) methods,^{30–32} which treats light atomic nuclei such as protons and deuterons as quantum wavefunctions, similar to electrons. The MC_QM method allows electronic structures to reflect the NQEs. Several methods that also can also incorporate the NQEs into electronic structure calculations have been developed, such as the nuclear orbital plus molecular orbital (NOMO) methods^{33–35} by the Nakai group and the nuclear-electronic orbital (NEO) methods³⁶ by the Hammes-Schiffer group, among others. Therefore, the MC_QM method enables convenient expression of changes due to the NQEs on the geometrical parameters. To date, we have applied the MC_QM method to analyze the NQEs and deuterium isotope effects (H/D isotope effects) in various proton transfer reactions,^{37–41} including excited-state intramolecular proton transfer.³⁸

In the excited-state, the PT reactions of 7-HQ mediated by solvent molecules involve multiple hydrogen bonds and multiple PTs, making the impact of NQEs of hydrogen nuclei considerable. However, calculations considering these NQEs have been limited thus far. Therefore, in this study, we analyzed the ESMPT mediated by three solvent MeOH molecules in 7-HQ using the MC_QM method to accurately incorporate the NQEs of hydrogen nuclei. We also analyzed the H/D isotope effects on the ESMPT in 7-HQ.

2. Multi-component methods

Here, we would like to introduce the basic outline of the multi-component methods. Detailed information can be found in literatures.^{30–32}

The total Hamiltonian for a system containing N_e -electrons, N_p -quantum hydrogen nuclei, and M -classical nuclei as utilized in the multi-component method is given as

$$\begin{aligned} \hat{H}_{\text{tot}} = & - \sum_i^{N_e} \frac{1}{2} \nabla_i^2 - \sum_i^{N_e} \sum_A^M \frac{Z_A}{r_{iA}} + \sum_{i < j}^{N_e} \frac{1}{r_{ij}} - \sum_p^{N_p} \frac{1}{2M_p} \nabla_p^2 \\ & + \sum_p^{N_p} \sum_A^M \frac{Z_p Z_A}{r_{pA}} + \sum_{p < q}^{N_p} \frac{Z_p Z_q}{r_{pq}} - \sum_i^{N_e} \sum_p^{N_p} \frac{Z_p}{r_{ip}} + \sum_{A < B}^M \frac{Z_A Z_B}{R_{pq}}, \end{aligned} \quad (1)$$

where indices of i and j refer to electrons, p and q refer to quantum hydrogen nuclei, and A and B refer to classical nuclei. The first three terms are also included in the conventional electronic Hamiltonian. The fourth to sixth terms are the terms pertaining to the quantum hydrogen nuclei, similar to the first three terms for electrons. Since the fourth term contains the nuclear mass, the multi-component calculations can distinguish the isotopic species. The seventh term represents the Coulomb interaction between the electron and quantum nucleus, and the last term represents the nuclear repulsion between classical nuclei.

The total wavefunction of the ground-state, Ψ_0 , is represented by a simple product of electronic (Φ_0^e) and nuclear (Φ_0^n) wavefunctions in the multi-component method,

$$\Psi_0 = \Phi_0^e \Phi_0^n. \quad (2)$$

The effective one-particle operators for electron and quantum nucleus are given as

$$\hat{f}_e = \hat{h}_e + \sum_i^{N_e} \hat{J}_i - \sum_p^{N_p} \hat{J}_p + V_{\text{XC}(ee)}, \quad (3)$$

$$\hat{f}_p = \hat{h}_p + \sum_p^{N_p} \hat{J}_p - \sum_i^{N_e} \hat{J}_i \quad (4)$$

where \hat{h}_e and \hat{h}_p are the one-particle operators for electron and quantum nucleus, \hat{J}_i and \hat{J}_p are the Coulomb operators for electron and quantum nucleus, respectively. $V_{\text{XC}(ee)}$ is the exchange–correlation term for electrons, and it can be evaluated using standard exchange–correlation functionals for electrons, such as B3LYP, M06 series, ω B97XD, and so on. Although quantum-mechanical treatment of nuclei gives rise to correlation term for electron–nucleus and exchange–correlation term for nuclei, their contributions are negligibly small in molecular systems. Thus, only $V_{\text{XC}(ee)}$ was evaluated in the present study. In current implementation, NQEs are directly considered only in the self-consistent field calculation. Excited-state properties are then calculated using the conventional TD-DFT procedures⁴² with the orbitals affected by the NQEs.

3. Computational details

Geometry-optimization calculations in the ground-state (GS) and S_1 excited-state (ES) were carried out using B3LYP/6-31+G(d,p) and TD-B3LYP/6-31+G(d,p) methods, respectively. All stationary point structures were characterized by normal mode analysis, and intrinsic reaction coordinate calculations were also conducted to confirm the connections between energy-minimum structures and transition state (TS) structures. Three MeOH molecules were explicitly included in the systems to describe the solvent-assisted PT.⁹ For comparison purposes, we also analyzed the PT reaction in 7-HQ mediated by two MeOH molecules. The solvent effects arising from other surrounding solvent molecules were considered by the IEFPCM model⁴³ implemented in Gaussian16.⁴⁴

The B3LYP- and TD-B3LYP-optimized structures were used as the initial structures for the subsequent MC_B3LYP and MC_TD-B3LYP calculations. In the MC_B3LYP and MC_TD-B3LYP calculations, only the migrating proton (deuteron) was treated as quantum wavefunction. Therefore, only the migrating hydrogen atom was replaced with a deuterium atom in the deuterated species. Hereafter, we will refer to the results for non-deuterated species as MC_B3LYP(H) and the results for deuterated species as MC_B3LYP(D). A single s-type Gaussian type function, $\psi = N \exp(-\alpha r^2)$, was adopted as the nuclear basis function, where N is the normalization constant and α is the orbital exponent value, which determines the spatial distribution of the nuclear wavefunction. Small and large α values represent diffusive and localized wavefunctions, respectively. Reasonable values of α are 24.1825 and 35.6214 for proton and

deuteron, respectively.^{45,46} Similar to the conventional (TD-)DFT calculations, all stationary point structures obtained by MC_(TD-)DFT calculations were characterized by normal mode analysis.

All calculations were performed with the modified version of Gaussian16 program package.

4. Results and discussions

4.1. Energy profiles for the proton transfer reaction in 7-HQ in the ground-state and S_1 excited-state obtained by the conventional B3LYP and TD-B3LYP calculations

Fig. 1 shows the relative potential energy profiles for the PT reactions in 7-HQ mediated by three MeOH solvent molecules (7-HQ + 3MeOH) in the GS and S_1 ES obtained by the B3LYP/6-31+G(d,p) and TD-B3LYP/6-31+G(d,p) calculations. The enol form was more stable than the keto form in the GS. The enol and keto forms were connected by a single TS, indicating that the GSPT reaction in 7-HQ proceeded in a concerted fashion. The activation barrier was 16.8 kcal mol⁻¹ for 7-HQ + 3MeOH. It is important to note that the activation barrier for 7-HQ with two MeOH molecules (7-HQ + 2MeOH) was 23.6 kcal mol⁻¹ (see, Table S1 in SI) at the same level of calculations, indicating that the third MeOH molecule plays a crucial role in the GSPT in 7-HQ. In contrast, in the S_1 ES, the keto form was more stable than the enol form. The ESPT also proceeded in a concerted fashion, similar to the GSPT. The activation barrier for the ESPT was 5.1 kcal mol⁻¹, which was much lower than the barrier for the GSPT. Therefore, our calculations revealed that the third MeOH molecule plays a significant role in the PT process in both the GS and ES, aligning with Matsumoto's conclusion based on experimental studies.⁹

Next, we would like to shed light on the NQEs on the relative potential energy profiles of 7-HQ + 3MeOH. Relative energies for enol, TS, and keto forms obtained by MC_B3LYP and MC_TD-B3LYP calculations were also listed in Table 1. Significant changes were observed in the activation barriers for both GSPT and ESPT reactions. While the B3LYP calculation gave an activation barrier of 16.8 kcal mol⁻¹ for the GSPT, the activation barrier calculated by

Table 1 Relative energies [kcal mol⁻¹] of enol and keto forms in the ground-state (S_0) and first excited-state (S_1) of 7-HQ with three MeOH molecules, calculated using MC_(TD-)B3LYP and (TD-)B3LYP methods

	MC_B3LYP(H)	MC_B3LYP(D)	B3LYP
S_0 enol	0.0	0.0	0.0
S_0 TS	9.2	11.3	16.8
S_0 keto	6.2	6.5	6.8
S_0 keto (S_1 geom)	14.7	15.0	15.6
S_1 enol (Frank-Condon)	84.3	85.0	86.5
S_1 enol	77.2 (0.0) ^a	78.3 (0.0) ^a	80.5 (0.0) ^a
S_1 TS	77.6 (0.4) ^a	79.6 (1.3) ^a	85.6 (5.1) ^a
S_1 keto	66.1 (-11.1) ^a	65.9 (-12.4) ^a	65.6 (-14.9) ^a

^a Values in parenthesis are the energies relative to S_1 enol form.

MC_B3LYP(H), which includes the NQEs of protons, was 9.2 kcal mol⁻¹, showing a reduction of 7.6 kcal mol⁻¹. Similarly, the activation barrier for the deuterated system (MC_B3LYP(D)) was 11.3 kcal mol⁻¹, showing a reduction of 5.5 kcal mol⁻¹. Since a deuteron is twice as heavy as a proton, the NQEs of deuterons are weaker than those of protons. These differences in the NQEs explain the smaller reduction observed in the MC_B3LYP(D) result compared to the MC_B3LYP(H) result. The NQEs also reduced the activation barriers in the ESPT. The activation barriers in the MC_B3LYP(H) and MC_B3LYP(D) results were 0.4 kcal mol⁻¹ and 1.3 kcal mol⁻¹, respectively. Thus, the activation barriers became negligibly small at room temperature by considering the NQEs of protons and deuterons.

These results clearly demonstrate the significance of the NQEs of protons in the analysis of GSPT and ESPT reactions. The NQEs affect not only energy profiles but also the optimized geometries and the electronic state of the molecules. We will analyze the NQEs on these properties in the following sections.

4.2. Nuclear quantum and H/D isotope effects on the geometrical parameters and atomic charge densities in 7-HQ in the ground-state and S_1 excited-state obtained by the MC_B3LYP and MC_TD-B3LYP calculations

Fig. 2 shows the optimized structures of enol, TS, and keto structures of 7-HQ + 3MeOH in the GS obtained by (MC_)B3LYP/

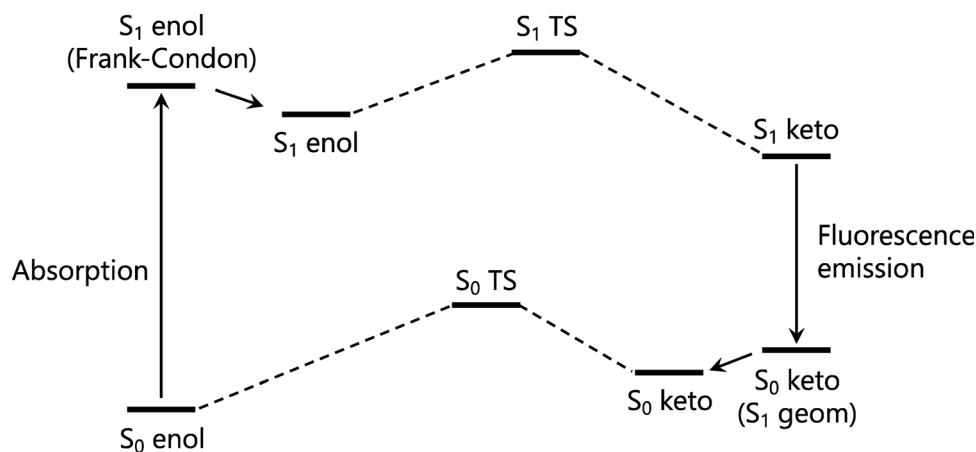


Fig. 1 Potential energy profiles for the ground-state and excited-state proton transfer reactions in 7-HQ obtained by (TD-)B3LYP and MC_(TD-)B3LYP calculations.



Fig. 2 Enol, TS, and keto structures of 7-HQ + 3MeOH in the ground-state optimized by (MC_)B3LYP/6-31+G(d,p) calculations.

6-31+G(d,p) calculations. The representative interatomic distances and Mulliken charge densities in the enol and keto forms at the GS are listed in Table 2. In both forms, the covalent X–H (X = O or N) bond distances were elongated, while hydrogen-bonded distances and distance between heavy atoms were shortened due to the inclusion of the NQEs. The elongations of the covalent bond distances were due to the direct inclusion of the anharmonicity of the potential energy curve along the covalent bond direction, as accounted for by the MC_B3LYP method.

Meanwhile, the shortenings observed in the hydrogen-bonded distances and distances between heavy atoms could not be explained by the anharmonicity of the potential energy curve, but could be explained by the changes in Mulliken charges for the atoms participating in the hydrogen-bond network. As shown in Table 2, negative charges of oxygen and nitrogen atoms and positive charges of hydrogen atoms were enhanced by the NQEs, resulting in the strengthening of the hydrogen-bond interactions.

The interatomic distances and Mulliken charge densities in the enol and keto forms at the S_1 ES are listed in Table 3. First,

we focus on the geometrical parameters in the enol form at the S_1 ES. The hydrogen-bonded distances in the S_1 ES were clearly shorter than those in the GS, indicating that the electronic excitation strengthened the hydrogen-bond interactions, thereby facilitating the ESPT reaction. In addition, the NQEs induced the same trends of changes in geometrical parameters as in the GS; they elongated the covalent bond distances while shortening the hydrogen-bonded distances. Thus, it can be inferred that the negligibly small activation barriers for the ESPT in 7-HQ on the MC_B3LYP(H) and MC_B3LYP(D) S_1 potential energy surfaces result from the combined effects of electronic excitation and the inclusion of NQEs.

4.3. Nuclear quantum and H/D isotope effects on energy profiles for the intramolecular proton transfer reaction in 7-hydroxyquinoline in the ground-state and S_1 excited-state obtained by the MC_B3LYP and MC_TD-B3LYP calculations

Next, we analyzed the absorption and fluorescence properties of 7-HQ + 3MeOH (Table 4). The TD-B3LYP calculations were

Table 2 Representative interatomic distances [Å] and Mulliken atomic charges in the enol, TS, and keto structures in the GS obtained by MC_B3LYP and B3LYP calculations

	Enol			TS			Keto		
	MC_B3LYP		B3LYP	MC_B3LYP		B3LYP	MC_B3LYP		B3LYP
	H	D		H	D		H	D	
$R(\text{O1-H1})$ [Å]	1.039	1.026	0.999	1.209	1.176	1.103	1.488	1.539	1.623
$R(\text{H1-O2})$ [Å]	1.557	1.586	1.652	1.232	1.262	1.343	1.059	1.040	1.007
$R(\text{O2-H2})$ [Å]	1.031	1.019	0.993	1.226	1.202	1.144	1.513	1.572	1.661
$R(\text{H2-O3})$ [Å]	1.583	1.615	1.686	1.206	1.223	1.275	1.047	1.028	0.997
$R(\text{O3-H3})$ [Å]	1.029	1.017	0.992	1.280	1.291	1.370	1.530	1.579	1.666
$R(\text{H3-O4})$ [Å]	1.596	1.629	1.699	1.161	1.147	1.083	1.044	1.028	0.997
$R(\text{O4-H4})$ [Å]	1.038	1.026	1.000	1.334	1.363	1.476	1.573	1.617	1.698
$R(\text{H4-N})$ [Å]	1.655	1.682	1.741	1.200	1.174	1.103	1.093	1.077	1.045
$q(\text{H1})$	0.502	0.497	0.480	0.542	0.545	0.544	0.499	0.483	0.460
$q(\text{H2})$	0.498	0.491	0.471	0.544	0.543	0.541	0.514	0.504	0.481
$q(\text{H3})$	0.504	0.497	0.476	0.542	0.541	0.534	0.509	0.501	0.480
$q(\text{H4})$	0.477	0.472	0.455	0.510	0.505	0.477	0.462	0.446	0.418
$q(\text{O1})$	-0.585	-0.584	-0.583	-0.646	-0.640	-0.620	-0.654	-0.640	-0.634
$q(\text{O2})$	-0.669	-0.664	-0.647	-0.736	-0.744	-0.757	-0.697	-0.670	-0.642
$q(\text{O3})$	-0.697	-0.690	-0.670	-0.746	-0.758	-0.804	-0.695	-0.698	-0.675
$q(\text{O4})$	-0.639	-0.635	-0.620	-0.695	-0.702	-0.711	-0.667	-0.658	-0.643
$q(\text{N})$	-0.230	-0.229	-0.225	-0.254	-0.248	-0.215	-0.207	-0.181	-0.183

Table 3 Representative interatomic distances [Å] and Mulliken atomic charges in the enol, TS, and keto structures in the S₁ ES obtained by MC_TD-B3LYP and TD-B3LYP calculations

	Enol			TS			Keto		
	MC_TD-B3LYP			MC_TD-B3LYP			MC_TD-B3LYP		
	H	D	TD-B3LYP	H	D	TD-B3LYP	H	D	TD-B3LYP
<i>R</i> (O1–H1) [Å]	1.122	1.085	1.033	1.209	1.257	1.356	1.577	1.606	1.670
<i>R</i> (H1–O2) [Å]	1.339	1.397	1.496	1.226	1.176	1.094	1.033	1.021	0.995
<i>R</i> (O2–H2) [Å]	1.069	1.043	1.004	1.129	1.147	1.187	1.551	1.583	1.651
<i>R</i> (H2–O3) [Å]	1.437	1.496	1.596	1.322	1.287	1.219	1.034	1.021	0.996
<i>R</i> (O3–H3) [Å]	1.066	1.041	1.004	1.105	1.102	1.076	1.562	1.593	1.662
<i>R</i> (H3–O4) [Å]	1.448	1.505	1.605	1.368	1.365	1.389	1.032	1.020	0.994
<i>R</i> (O4–H4) [Å]	1.095	1.066	1.022	1.136	1.126	1.080	1.629	1.658	1.722
<i>R</i> (H4–N) [Å]	1.482	1.536	1.630	1.408	1.416	1.477	1.077	1.065	1.038
<i>q</i> (H1)	0.548	0.541	0.518	0.542	0.538	0.522	0.487	0.479	0.458
<i>q</i> (H2)	0.530	0.518	0.488	0.555	0.561	0.573	0.511	0.501	0.476
<i>q</i> (H3)	0.529	0.517	0.489	0.551	0.555	0.561	0.594	0.496	0.474
<i>q</i> (H4)	0.505	0.497	0.475	0.503	0.501	0.492	0.450	0.440	0.412
<i>q</i> (O1)	−0.549	−0.541	−0.527	−0.565	−0.576	−0.591	−0.584	−0.584	−0.584
<i>q</i> (O2)	−0.704	−0.698	−0.677	−0.702	−0.699	−0.689	−0.690	−0.682	−0.658
<i>q</i> (O3)	−0.715	−0.703	−0.675	−0.757	−0.762	−0.760	−0.698	−0.689	−0.663
<i>q</i> (O4)	−0.686	−0.678	−0.654	−0.698	−0.700	−0.695	−0.668	−0.662	−0.644
<i>q</i> (N)	−0.348	−0.346	−0.334	−0.323	−0.324	−0.334	−0.223	−0.223	−0.220

performed at the GS enol and the ES keto forms to investigate the absorption and fluorescence properties, respectively. The calculated absorption and fluorescence peak appeared at 330 nm and 569 nm, respectively, by the TD-B3LYP calculation. It should be noted here that the experimental values are $\lambda^{\text{abs}} = 320$ nm and $\lambda^{\text{flu}} = 500$ –520 nm.⁶ The TD-B3LYP calculations slightly overestimated the experimental values, but the results were still in reasonable agreement with the experimental data.

The absorption and fluorescence peak positions are also affected by the NQEs of the protons and deuterons. The λ^{abs} values were 339 nm and 336 nm by the MC_TD-B3LYP(H) and MC_TD-B3LYP(D) calculations, respectively. The NQEs caused modest red shifts. On the other hand, the NQEs caused modest blue shifts of the fluorescence peak positions. The λ^{flu} values were 556 nm and 562 nm by the MC_TD-B3LYP(H) and MC_TD-B3LYP(D), respectively. The NQEs caused the absorption peaks to slightly deviate from the experimental value (320 nm). However, the fluorescence peaks were slightly shifted to the shorter wavelength region and brought closer to the experimental value by including the NQEs. Consequently, the calculated Stokes shift (217 nm for MC_B3LYP(H)) was closer to the experimental value (180–200 nm) compared to that estimated by the B3LYP

calculation (242 nm). Therefore, direct treatment of the NQEs is important to theoretically analyze the absorption and fluorescence properties of 7-HQ.

For both absorption and fluorescence of 7-HQ, the main contribution for the excitation is the HOMO–LUMO transition, and the coefficient for the HOMO–LUMO transition slightly increased as the NQEs of the migrating hydrogen nuclei increased.

Fig. 3 shows the Frontier orbitals (highest occupied molecular orbital (HOMO) and lowest unoccupied molecular orbital (LUMO)), and Table 5 lists the HOMO and LUMO energies and the differences between them (HOMO–LUMO energy gap, ΔHL) at the GS enol and at ES keto forms. The HOMO and LUMO consist of π (π^*) orbitals of 7-HQ. The ΔHL values in the GS enol form decreased as the NQEs of the hydrogen nucleus increased, whereas the gap in the ES keto form increased. Thus, the NQEs of the migrating proton or deuteron altered the molecular orbital energies, resulting in changes in the ΔHL values and the peak positions. Inoue and coworkers have studied the applicability of MC_QM methods for electronic excitation calculations. They conducted detailed analyses of NQEs in electronic excitations, especially in H₂O, HDO, and D₂O molecules, and revealed that the NQEs alter the shapes and characteristics of molecular orbitals.⁴⁷ Following Inoue's study, we also investigated the NQEs for electronic excitations in detail. We performed two types of additional calculations: (i) MC_B3LYP single-point calculation at the conventional B3LYP geometry, and (ii) B3LYP single-point calculation at the MC_B3LYP geometry. The former provides insight into how the quantum nature of protons itself alters the molecular orbital energies, whereas the latter clarifies how important the geometrical relaxations induced by the NQEs are. As shown in Tables S2 and S3 in SI, unlike the case of electronic excitations in H₂O, HDO, and D₂O, the geometrical relaxation effects are clearly dominant for the HOMO–LUMO excitation in 7-HQ. This seems

Table 4 Absorption and fluorescence properties of 7-HQ + 3MeOH calculated by MC_TD-B3LYP and TD-B3LYP calculations

	Method	λ (nm)	Contribution	Coefficient
Absorption	MC_TD-B3LYP(H)	339	HOMO → LUMO	0.6863
	MC_TD-B3LYP(D)	336	HOMO → LUMO	0.6858
	TD-B3LYP	330	HOMO → LUMO	0.6846
	Exp. ⁶	320		
Emission	MC_TD-B3LYP(H)	556	HOMO → LUMO	0.6948
	MC_TD-B3LYP(D)	562	HOMO → LUMO	0.6946
	TD-B3LYP	572	HOMO → LUMO	0.6943
	Exp. ⁶	500–520		



Fig. 3 The frontier molecular orbitals of 7-HQ at (a) the GS enol and (b) the ES keto forms.

Table 5 HOMO and LUMO energies [eV] and HOMO–LUMO energy gap (Δ H) [eV] at GS enol and ES keto structures

	Enol (GS)			Keto (ES)		
	$E(\text{HOMO})$	$E(\text{LUMO})$	ΔHL^a	$E(\text{HOMO})$	$E(\text{LUMO})$	ΔHL^a
MC_B3LYP(H)	−6.113	−1.927	4.186	−5.384	−2.594	2.790
MC_B3LYP(D)	−6.139	−1.920	4.219	−5.374	−2.607	2.767
B3LYP	−6.192	−1.906	4.286	−5.356	−2.632	2.724

$$^a \Delta\text{HL} = E(\text{LUMO}) - E(\text{HOMO}).$$

reasonable because the HOMO and LUMO in 7-HQ consist of π and π^* orbitals localized on the molecular plane of 7-HQ, so the NQEs of the protons/deuterons may not directly affect the electronic excitation properties. Therefore, these analyses demonstrate that even if the molecular orbitals related to the excitation do not include contributions from the protons/deuterons, the NQEs of protons/deuterons can still alter the molecular orbital energies indirectly through geometrical relaxation.

Δ HL values became smaller and larger as the NQE increased at the GS enol and ES keto structures, respectively. Since HOMO–LUMO transition was the main contribution for both absorption and fluorescence, the changes in the Δ HL values induced the changes in the absorption and fluorescence properties.

5. Conclusion

In this study, the solvent (MeOH) mediated PT reaction in 7-HQ was thoroughly investigated by DFT calculations. We mainly focused on the NQEs on the energy profiles of the reaction, the

optimized geometrical parameters, and absorption and fluorescence properties. Our analyses were conducted with the aid of the MC_DFT method, which can directly include the NQEs of protons and deuterons. Our MC_DFT calculations revealed that the NQEs induced elongation of the covalent N–H/O–H bond lengths and contraction of the hydrogen-bonded H \cdots N/H \cdots O distances and the distances between heavy atoms (O \cdots N) even in the electronic S_1 excited-state.

The NQEs of proton and deuteron induced not only geometrical changes but also the changes in orbital energies. As a result, the HOMO–LUMO energy gap values and absorption/fluorescence properties were also affected by the NQEs. The MC_TD-B3LYP(H) calculation predicted the Stokes shift as 217 nm, which is closer to the experimental value (180–200 nm) compared to the TD-B3LYP calculation. Therefore, the present study clearly demonstrated that the NQEs of protons and deuterons are important for representing not only H/D isotope effects but also absorption and fluorescence properties.

Conflicts of interest

There are no conflicts to declare.

Data availability

Supplementary information is available. See DOI: <https://doi.org/10.1039/d5cp02666k>.

The data supporting the findings of this study are presented in the main text and SI.

Acknowledgements

This work was financially supported by JSPS KAKENHI Grant No. 22H02141 (to T. U.), No. 21H00026 and 23K17905 (to M. T.), No. 25K08559 (to T. U., and Y. K.) and No. 25H00428 (T. U., T. I., and M. T.). The generous allotment of computational time from the Research Center for Computational Science, Okazaki, Japan (Project No: 24-IMS-C349 and 25-IMS-C299 to T. U.), is also gratefully acknowledged.

References

- 1 *An Introduction to Hydrogen Bonding*, ed. G. A. Jeffery, Oxford University Press, New York, 1997.
- 2 S. Horiuchi, Y. Tokunaga, G. Giovannetti, S. Picozzi, H. Itoh, R. Shimano, R. Kumai and Y. Tokura, *Nature*, 2010, **463**, 789–792.
- 3 N. Agmon, *Chem. Phys. Lett.*, 1995, **244**, 456–462.
- 4 T. Kumagai, A. Shiotari, H. Okuyama, S. Hatta, T. Aruga, I. Hamada, T. Frederiksen and H. Ueba, H-atom relay reactions in real space, *Nat. Mater.*, 2012, **11**, 167–172.
- 5 H. Fang and Y. Kim, *Theor. Chem. Acc.*, 2017, **136**, 28.
- 6 Y. Cui, H. Zhao, J. Zhao, P. Li, P. Song and L. Xia, *New J. Chem.*, 2015, **39**, 9910–9917.

- 7 M. Guglielmi, I. Tavernelli and U. Rothlisberger, *Phys. Chem. Chem. Phys.*, 2009, **11**, 4549–4555.
- 8 C. Tanner, C. Manca and S. Leutwyler, *Science*, 2003, **302**, 1736–1739.
- 9 Y. Matsumoto, T. Ebata and N. Mikami, *J. Phys. Chem. A*, 2002, **106**, 5591–5599.
- 10 W.-H. Fang, *J. Am. Chem. Soc.*, 1998, **120**, 7568–7576.
- 11 M. I. Avadanei, R. I. Tigoianu and O. G. Avadanei, *J. Photochem. Photobiol., A*, 2025, **459**, 116018.
- 12 S. Wang, W. Sun, H. Mu, J. Gao, X. Guan, H. Li, G. He and G. Jin, *J. Mol. Struct.*, 2025, **1321**, 140180.
- 13 Z. Tang, S. Wang, X. Wang, B. Fan, Q. Wei and J. Zhao, *J. Mol. Struct.*, 2025, **1319**, 139474.
- 14 X. Xin, W. Shi, R. Jia, G. Zhao, H. Zuang and Y. Li, *J. Mol. Struct.*, 2024, **1318**, 139328.
- 15 R. Salaeh, W. Inporn, W. Chansen, N. Kungwan and R. Daengngern, *Colloids Surf., A*, 2024, **697**, 134327.
- 16 S. Abou-Hatab and S. Matsika, *Phys. Chem. Chem. Phys.*, 2024, **26**, 4511–4523.
- 17 A. K. Shukla, D. S. Sisodiya, Savita, A. Chattopadhyay and A. Bhattacharya, *J. Phys. Chem. B*, 2023, **127**, 10025–10034.
- 18 Z. Li, Z. Tang, W. Li, H. Zhan, X. Liu, Y. Wang, J. Tian and X. Fei, *J. Mol. Liq.*, 2021, **341**, 116920.
- 19 F. Zhang, J. Zhao and C. Li, *J. Phys. Org. Chem.*, 2021, **34**, e4257.
- 20 D. Zheng, M. Zhang and G. Zhao, *Sci. Rep.*, 2017, **7**, 13766.
- 21 D. Stoner-Ma, A. A. Jaye, K. L. Ronayne, J. Nappa, S. R. Meech and P. J. Tonge, *J. Am. Chem. Soc.*, 2008, **130**, 1227–1235.
- 22 D. Marx, M. Tuckerman, J. Hutter and M. Parrinello, *Nature*, 1999, **397**, 601.
- 23 S.-Y. Park, Y.-S. Lee, O.-H. Kwon and D.-J. Jang, *Chem. Commun.*, 2009, 926.
- 24 P.-T. Chou, C.-Y. Wei, C.-R. C. Wang, F.-T. Hung and C.-P. Chang, *J. Phys. Chem. A*, 1999, **103**, 1939.
- 25 S.-Y. Park, B. Kim, Y.-S. Lee, O.-H. Kwon and D.-J. Jang, *Photochem. Photobiol. Sci.*, 2009, **8**, 1611.
- 26 S.-Y. Park and D.-J. Jang, *J. Am. Chem. Soc.*, 2010, **132**, 297.
- 27 H. Lim, S.-Y. Park and D.-J. Jang, *J. Phys. Chem. A*, 2010, **114**, 11432.
- 28 B. Kang, K. C. Ko, S.-Y. Park, D.-J. Jang and J. Y. Lee, *Phys. Chem. Chem. Phys.*, 2011, **13**, 6332.
- 29 O.-H. Kwon, Y.-S. Lee, B. K. Yoo and D.-J. Jang, *Angew. Chem., Int. Ed.*, 2006, **45**, 415.
- 30 T. Udagawa, T. Tsuneda and M. Tachikawa, *Phys. Rev. A: At., Mol., Opt. Phys.*, 2014, **89**, 052519.
- 31 T. Udagawa and M. Tachikawa, *J. Chem. Phys.*, 2006, **125**, 244105.
- 32 M. Tachikawa, K. Mori, H. Nakai and K. Iguchi, *Chem. Phys. Lett.*, 1998, **290**, 437–442.
- 33 Y. Imamura, Y. Tsukamoto, H. Kiryu and H. Nakai, *Bull. Chem. Soc. Jpn.*, 2009, **82**, 1133–1139.
- 34 Y. Imamura, H. Kiryu and H. Nakai, *J. Comput. Chem.*, 2008, **29**, 735–740.
- 35 H. Nakai, *Int. J. Quantum Chem.*, 2001, **86**, 511–517.
- 36 F. Pavošević, T. Culpitt and S. Hammes-Schiffer, *Chem. Rev.*, 2020, **120**, 4222–4253.
- 37 T. Udagawa, H. Shibata and M. Tachikawa, *Chem. Phys.*, 2024, **581**, 112258.
- 38 T. Udagawa, I. Hattori, Y. Kanematsu, T. Ishimoto and M. Tachikawa, *Int. J. Quantum Chem.*, 2022, **122**, e26962.
- 39 T. Udagawa, R. B. Murphy, T. A. Darwish, M. Tachikawa and S. Mori, *Bull. Chem. Soc. Jpn.*, 2021, **94**, 1954–1962.
- 40 N. Yodsinsin, H. Sakagami, T. Udagawa, T. Ishimoto, S. Jungstittwong and M. Tachikawa, *Mol. Catal.*, 2021, **504**, 11486.
- 41 H. Funahashi, M. Tachikawa and T. Udagawa, *Org. Lett.*, 2020, **22**, 9439–9443.
- 42 M. E. Casida, C. Jamorski, K. C. Casida and D. R. Salahub, *J. Chem. Phys.*, 1998, **108**, 4439.
- 43 J. Tomasi, B. Mennucci and R. Cammi, *Chem. Rev.*, 2005, **105**, 2999–3093.
- 44 M. J. Frisch, G. W. Trucks, H. B. Schlegel, G. E. Scuseria, M. A. Robb, J. R. Cheeseman, G. Scalmani, V. Barone, G. A. Petersson, H. Nakatsuji, X. Li, M. Caricato, A. V. Marenich, J. Bloino, B. G. Janesko, R. Gomperts, B. Mennucci, H. P. Hratchian, J. V. Ortiz, A. F. Izmaylov, J. L. Sonnenberg, D. Williams-Young, F. Ding, F. Lipparini, F. Egidi, J. Goings, B. Peng, A. Petrone, T. Henderson, D. Ranasinghe, V. G. Zakrzewski, J. Gao, N. Rega, G. Zheng, W. Liang, M. Hada, M. Ehara, K. Toyota, R. Fukuda, J. Hasegawa, M. Ishida, T. Nakajima, Y. Honda, O. Kitao, H. Nakai, T. Vreven, K. Throssell, J. A. Montgomery, Jr., J. E. Peralta, F. Ogliaro, M. J. Bearpark, J. J. Heyd, E. N. Brothers, K. N. Kudin, V. N. Staroverov, T. A. Keith, R. Kobayashi, J. Normand, K. Raghavachari, A. P. Rendell, J. C. Burant, S. S. Iyengar, J. Tomasi, M. Cossi, J. M. Millam, M. Klene, C. Adamo, R. Cammi, J. W. Ochterski, R. L. Martin, K. Morokuma, O. Farkas, J. B. Foresman and D. J. Fox, *Gaussian 16, Revision C.01*, Gaussian, Inc., Wallingford CT, 2016.
- 45 T. Ishimoto, M. Tachikawa and U. Nagashima, *Int. J. Quantum Chem.*, 2006, **106**, 1465–1476.
- 46 T. Ishimoto, M. Tachikawa and U. Nagashima, *J. Chem. Phys.*, 2006, **125**, 144103.
- 47 M. Inoue, T. Ishimoto, D. S. R. Rocabado, T. Udagawa, M. Tachikawa, M. Baba and Y. Kanematsu, *Chem. Lett.*, 2025, **54**, upaf031.